ACS Catalysis

Research Article

pubs.acs.org/acscatalysis

Photocatalytic CO_2 Reduction with H_2O on TiO_2 Nanocrystals: Comparison of Anatase, Rutile, and Brookite Polymorphs and Exploration of Surface Chemistry

Lianjun Liu,[†] Huilei Zhao,[†] Jean M. Andino,[‡,§] and Ying Li*[,†]

[†]Department of Mechanical Engineering, University of Wisconsin-Milwaukee, Milwaukee, Wisconsin 53211, United States

[‡]Chemical Engineering and [§]Civil, Environmental, and Sustainable Engineering, Arizona State University, Tempe, Arizona 85287, United States

Supporting Information

ABSTRACT: CO_2 photoreduction with water vapor has been studied on three TiO_2 nanocrystal polymorphs (anatase, rutile, and brookite) that were engineered with defect-free and oxygen-deficient surfaces, respectively. It was demonstrated that helium pretreatment of the as-prepared TiO_2 at a moderate temperature resulted in the creation of surface oxygen vacancies (V_O) and Ti^{3+} sites on anatase and brookite but not on rutile. The production of CO and CH_4 from CO_2 photoreduction was remarkably enhanced on defective anatase and brookite TiO_2 (up to 10-fold enhancement) as compared to the defect-free surfaces. Defective brookite was photocatalytically more active than anatase and rutile, probably because of a lower formation energy of V_O on brookite. The results from in situ diffuse reflectance infrared Fourier transform spectroscopy (DRIFTS) analyses suggested that (1) defect-free TiO_2 was not active for CO_2 photoreduction since no CO_2^- is generated, and (2) CO_2 photoreduction to CO possibly underwent different reaction pathways on oxygen-deficient anatase and brookite via different intermediates (e.g., CO_2^- on anatase; CO_2^- and HCOOH on brookite). The combined DRIFTS and photoactivity studies reported in this paper have provided new insights to the role of surface defects in CO_2 photoreduction on TiO_2 nanocrystals, and revealed significant information on the much less studied but promising brookite phase.

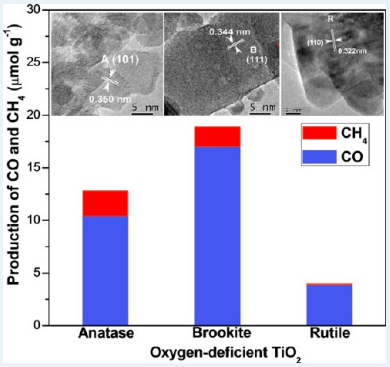

KEYWORDS: *CO_2 photoreduction, oxygen vacancy, TiO_2, Brookite, In situ DRIFTS*

1. INTRODUCTION

Photocatalytic reduction of CO_2 with H_2O on the inexpensive and environmentally benign TiO_2 is particularly interesting because it is a promising "green chemistry" approach for the direct conversion of CO_2 to value-added fuels (CO, methane, methanol, etc.) by sunlight.[1,2] TiO_2 naturally occurs as three polymorphs: anatase, brookite and rutile. Among them, only TiO_2 anatase, rutile, or anatase-rutile mixed phase (e.g., Evonik-Degussa P25) have been studied for CO_2 photoreduction, either as bare TiO_2[3−8] or with the modifications of incorporating metal (e.g., Pt),[9] nonmetal (e.g., N, I),[1,10] and metal oxide (e.g., CuO_x),[11,12] or TiO_2 dispersed on mesoporous silica support.[13,14] By contrast, the brookite phase is much less studied as a photocatalyst and has not been studied for CO_2 photoreduction so far, probably because of the previous difficulty in synthesizing high quality brookite nanocrystallites. Controversy also exists in the literature on the activity of the brookite phase. Kandiel et al.[15] revealed that anatase nanoparticles exhibited higher photoactivity than brookite or an anatase/brookite mixture for the photo-oxidation of dichloroacetic acid (DCA); whereas, Li et al.[16] demonstrated that brookite had the highest photoefficiency in the oxidation of methyl orange among the three phases, and Chiarello et al.[17] showed that brookite is as active as anatase in photocatalytic hydrogen production from water. This uncertainty in photoactivity and the lack of literature on CO_2 photoreduction over brookite TiO_2 motivated us to explore this rarely studied phase and the corresponding surface photochemistry.

The efficiency of CO_2 photoreduction with water by TiO_2 is generally very low. Therefore, advancing the CO_2 reduction process on TiO_2 remains a challenge. Besides the previously mentioned modification of the catalyst composition to enhance catalytic activity, the creation of defect disorder in TiO_2 has been reported to greatly influence its photoactivity,[18−20] because defects like oxygen vacancies (V_O) can serve as surface reactive sites (react with H_2O, for example) at the solid−solid interface,[21] and they can also donate excess unpaired electrons to Ti atoms that are subsequently reduced into Ti^{3+}. These stored electrons may strongly affect the surface chemistry and charge transport properties of TiO_2.[22] Theoretical calculations have revealed that the formation energies of V_O and Ti interstitial decrease by the order of rutile, anatase, and brookite, suggesting it is easiest to form surface defects on brookite

Received: April 27, 2012
Revised: July 12, 2012
Published: July 16, 2012

   dx.doi.org/10.1021/cs300273q | ACS Catal. 2012, 2, 1817−1828

TiO_2.[23] Analyses of the published literature led us to hypothesize that the creation of defective TiO_2 with V_O (particularly the defective nanostructured brookite) was one alternative way to promote the efficiency of CO_2 photoreduction.

The majority of the published experimental work on CO_2 photoreduction over TiO_2 used stoichiometric TiO_2 made by calcination in an air environment in the final step or without calcination. Only a few theoretical studies reported the interaction of CO_2 on oxygen-deficient TiO_{2-x} anatase or rutile.[24,25] One of the few experimental studies of CO_2 photoreduction on defective TiO_2 was recently conducted by DeSario et al.[26] who synthesized nonstoichiometric mixed phased TiO_{2-x} (anatase and rutile) thin films by direct current magnetron sputtering. They demonstrated that V_O enhanced visible light harvesting, and the improved activity depended on the concentration of V_O. However, how CO_2 was activated with V_O on anatase and rutile phase was not clearly addressed in that work. Our recent work investigated the activation mechanism of CO_2 on the defective surface of Cu-deposited TiO_2 (P25) nanoparticles, and demonstrated that the presence of V_O and Cu(I) species facilitated the spontaneous dissociation of CO_2 to CO both in the dark and under photoillumination.[27] So far, no research has been conducted to compare CO_2 photoreduction activity on perfect and oxygen-deficient TiO_2 anatase, rutile, and brookite nanocrystals, respectively, and to study the phase-dependent surface active sites and reaction mechanism.

The mechanism of CO_2 activation and reduction with H_2O on a photoexcited TiO_2 surface also remains very important. The adsorption of CO_2 and H_2O on TiO_2 is the preceding step of the photoreduction reactions; however, this important step has been scarcely studied. Only limited literature on the nature of CO_2 or H_2O chemisorption on TiO_2 has been reported using either theoretical calculations for single crystal TiO_2[21,24,28,29] or experimental measurements for powdered[14,30−32] and thin films of TiO_2.[21,25,33] The theoretical calculations indicated that electron transfer to CO_2 may only be mediated by surface defects like V_O,[34] and factors such as phase components (e.g., rutile, anatase) and surface defects would critically affect the H_2O-TiO_2 interaction.[29] In this work, we have applied a powerful tool, in situ diffuse reflectance infrared Fourier transform spectroscopy (DRIFTS), to identify the CO_2 adsorption species and reaction intermediates on the three TiO_2 polymorph surfaces. While there are a limited number of IR studies on the mechanism of CO_2 reduction on perfect TiO_2 surfaces with intermediates such as CO, formaldehyde, and bent-CO_2^- being reported,[14,30,32] the influence of surface defect sites on the reaction intermediates/pathways has not been experimentally investigated in the literature.

The present work systematically studied the photoreduction of CO_2 with H_2O on defect-free and defective TiO_2 anatase, rutile, and brookite nanocrystals, respectively, and compared the difference in their nanostructure, morphology, and photoactivity in CO_2 reduction. The role of surface active sites and the possible reaction mechanism/intermediates were also reported through the correlation of in situ DRIFTS studies with the photoactivity data.

2. EXPERIMENTAL SECTION

2.1. Description of the DRIFTS System. All IR spectra presented in this work were recorded on a Nicolet 6700 spectrometer (Thermo Electron) equipped with a liquid nitrogen cooled HgCdTe (MCT) detector. The spectra were displayed in absorbance units, and acquired with a resolution of 4 cm^{-1}, using 32 scans. The in situ DRIFTS studies were performed in a Praying Mantis DRIFTS accessory and a reaction chamber (Harrick Scientific, HVC-DRP), as shown in Figure 1. The dome of the cell has two KBr windows allowing

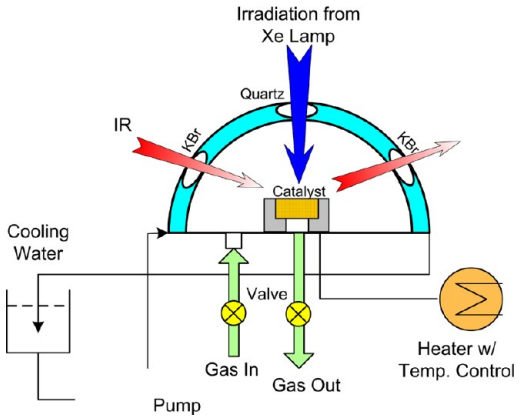

Figure 1. Schematic diagram of the in situ DRIFTS setup.

IR transmission and a third quartz window allowing transmission of irradiation introduced through a liquid light guide (Newport) that connects to a 450 W Xe arc system (Oriel). The light spectrum of the Xe lamp can be found in our previous work.[10]

2.2. Catalyst Preparation. TiO_2 nanocrystals in three phases were selectively prepared by hydrolysis and hydrothermal methods according to the literature.[15,35] To synthesize rutile TiO_2, titanium tetrachloride ($TiCl_4$) was added dropwise into ethanol under stirring. A transparent yellowish sol was formed, and then slowly added to distilled water under stirring. The molar ratio of $TiCl_4$, ethanol, and water was 2:20:280. After the addition was finished, the solution was further stirred for 30 min, and then was maintained in a closed system at 50 °C in an oven for 24 h. The white precipitate was harvested by centrifugation, and washed with distilled water and dried in an oven at 50 °C.

To prepare anatase TiO_2, 10 mL of titanium bis(ammonium lactate) dihydroxide (TALH) aqueous solution (50%) and a desired amount of 0.1 M urea were mixed followed by the addition of distilled water to reach a final volume of 100 mL. The resulting solution was transferred into a Teflon-lined autoclave, which was sealed and placed in an electric oven held at 160 °C for 24 h. Then, the autoclave was naturally cooled in air. The precipitates were separated by centrifugation, washed with distilled water until pH 7, and dried overnight at 60 °C in an oven. To prepare brookite TiO_2, a similar procedure was performed, but the concentration of urea was changed to 7 M. All three powders were calcined at 400 °C for 3 h at a heating rate of 2 °C/min.

To prepare oxygen-deficient TiO_2, the as-prepared TiO_2 samples were pretreated inside the DRIFT reaction cell (for investigation of CO_2 and H_2O interaction on TiO_2 surface) or inside the photoreactor (for activity tests of CO_2 photoreduction with H_2O) at 220 °C for 1.5 h with a flow of He (99.999%, 120 mL/min). The unpretreated and He pretreated TiO_2 samples were denoted as Ti(UP) and Ti(He), respectively, and the three polymorphs, that is, anatase, brookite, and rutile, were denoted as TiA(UP), TiB(UP), TiR(UP), TiA(He), TiB(He), and TiR(He), respectively.

2.3. Catalyst Characterization. The surface area, pore size, and pore volume of the unpretreated and pretreated TiO_2 samples were analyzed by nitrogen adsorption at 77 K with the Brunauer–Emmett–Teller (BET) method (Micromeritics, ASAP 2020). The crystal structures of the unpretreated and pretreated TiO_2 were identified by X-ray diffraction (XRD, Scintag XDS 2000) using Cu Kα irradiation at 45 kV and a diffracted beam monochromator at 40 mA. The crystal size of TiO_2 was calculated using the Scherer equation. Raman spectroscopy was carried out on a Renishaw 1000B system in the range of 100–1500 cm^{-1}. The lattice structures of individual nanocrystals were visualized by phase-contrast high resolution transmission electron microscopy (HRTEM) carried out with 300 keV electrons in a Hitachi H9000NAR instrument with 0.18 nm point and 0.11 nm lattice resolution. Amplitude contrast TEM images were used to obtain information about the sizes and morphology. UV–visible diffuse reflectance spectra (UV–vis DRS) were obtained by a UV–visible spectrometer (Ocean Optics) using $BaSO_4$ as the background. The state of Ti on TiO_2 samples was identified with DRIFTS by examining the characteristic Ti–OH bonds.

2.4. In situ DRIFTS Analyses for CO_2 Photoreduction with H_2O. In situ DRIFTS spectra of CO_2 photoreduction with H_2O vapor were recorded for unpretreated and in situ pretreated anatase and brookite TiO_2 samples. In the cases of TiA(UP) and TiB(UP), each sample was purged with He for 1 h at 25 °C, and a background spectrum in the presence of the sample was collected. After that, 10%CO_2/He (99.999%, Praxair) was continuously passed through a water bubble to bring a mixture of CO_2 and H_2O vapor into the chamber at 2.0 mL/min for 15 min. Subsequently, the inlet and outlet valves of the DRIFTS reaction cell were closed, and the sample was subjected to photoillumination for 90 min. In the cases of TiA(He) and TiB(He), the same procedure was used to obtain the IR spectra except that the sample underwent the previously described He-pretreatment process at 220 °C and the DRIFTS reaction cell was allowed to cool down to 25 °C before the IR spectra were taken.

2.5. Activity of CO_2 Photoreduction. The experiments of CO_2 photoreduction with H_2O on Ti(UP) and Ti(He) were carried out in a photoreactor similar to that reported in our previous study.[10] CO_2 (99.999%, Praxair) was continuously passed through a water bubbler to allow a mixture of CO_2 and H_2O vapor ($H_2O \approx 2.3$ v/v%) to traverse the photocatalyst-loaded glass fiber filter inside the photoreactor. A 150 W solar simulator (Oriel) was used as the excitation source, and the spectrum is shown in Supporting Information, Figure S1. The light intensity of the solar simulator was ~90 mW/cm^2 in the range of 200–1000 nm. As compared to the AM 1.5G standard, the solar simulator had a higher intensity in the UV range ($200 < \lambda < 400$ nm), but a lower intensity in the visible range ($400 < \lambda < 800$ nm). The photoreactor was operated in a continuous-flow mode (2.0 mL/min flow rate), and the gaseous products in the reactor effluent were continuously analyzed for 6 h by a gas chromatograph (GC, Agilent 7890A) equipped with both a thermal conductivity detector (TCD) and a flame ionization detector (FID). For each test, 100 mg of TiO_2 was used. For the Ti(He) samples, after the in situ pretreatment, the reactor was naturally cooled down to room temperature before the subsequent photoactivity measurement was conducted.

3. RESULTS

3.1. Crystal Structure and Textual Property of TiO_2 Polymorphs. The crystal structures of the prepared materials were confirmed by XRD and Raman spectroscopy. Figure 2a shows the XRD patterns of the as-prepared TiO_2. TiA(UP) remains in the pure anatase phase (JCPDS No. 21-1272, tetragonal) at 25.3, 37.8, and 47.9° (2θ). The diffraction peaks of TiR(UP) at 27.5, 36.1, 41.2, and 54.4° (2θ) are well indexed to the typical rutile (JCPDS No. 21-1276, tetragonal). The XRD pattern of TiB(UP) shows the discernible brookite phase

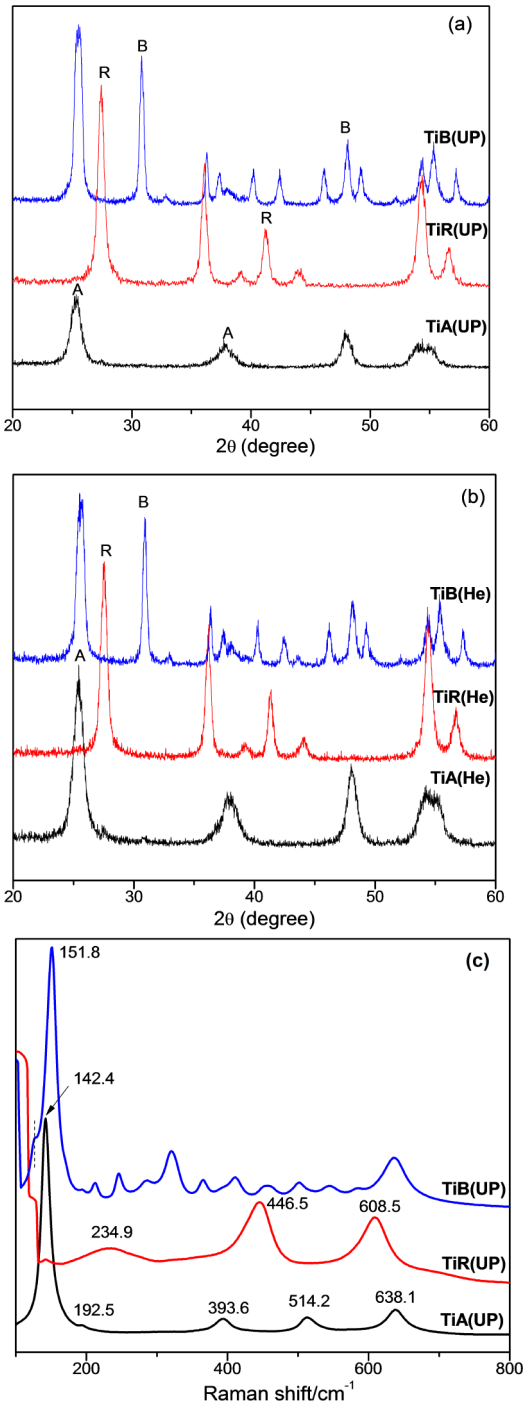

Figure 2. XRD patterns for (a) unpretreated and (b) He pretreated TiO_2; and (c) Raman spectra for unpretreated TiO_2 (anatase, rutile, and brookite).

dx.doi.org/10.1021/cs300273q | ACS Catal. 2012, 2, 1817–1828

(JCPDS No. 29-1360, orthorhombic) from its unique and strong (121) diffraction located at 30.80° (2θ). Pure brookite was obtained, although a very small fraction of amorphous TiO_2 was detected by the HRTEM analyses shown in a later section of this paper. In addition, TiR(UP) and TiB(UP) exhibited similar crystal sizes (11.5 and 11.0 nm, respectively), which were slightly larger than that of TiA(UP) (8.0 nm) (See Table 1). Figure 2b shows the XRD patterns of the pretreated TiO_2 samples. The diffraction peaks and crystal sizes of TiB(He) and TiR(He) (10.9 and 11.8 nm, respectively) were almost identical to those of TiB(UP) and TiR(UP). The TiA(He) sample remained as a pure anatase phase material. The diffraction peaks of TiA(He) appeared to be sharper than that of TiA(UP) as the crystal size of TiA(He) slightly increased from 8.0 to 8.8 nm (see Table 1). These results indicated that neither the crystal phases nor the crystal sizes of TiO_2 were significantly influenced by the He pretreatment at a moderate temperature (220 °C).

Table 1. Crystal Size, BET Surface Area, Pore Size, Pore Volume, and Space Group of the As-Prepared (Unpretreated) and Pretreated TiO_2 Samples

samples	crystallite size (nm)	BET surface area (m^2/g)	pore size (nm)	pore volume (cm^3/g)	space group
TiA(UP)	8.0	145.6	6.2	0.23	*I*41/*amd*
TiR(UP)	11.5	46.5	10.7	0.12	*P*42/*mnm*
TiB(UP)	11.0	76.6	18.4	0.35	*Pcab*
TiA(He)	8.8	163.8	4.7	0.19	*I*41/*amd*
TiR(He)	11.8	36.3	11.6	0.11	*P*42/*mnm*
TiB(He)	10.9	87.8	12.1	0.26	*Pcab*

In agreement with XRD results, Raman spectra of TiA(UP) and TiR(UP) in Figure 2c exhibited five characteristic Raman-active modes for anatase and three for the rutile phase.[16,36] The rich scenario of signals on TiB(UP) were related to the 36 Raman-active modes of a typical brookite phase, similar to the natural and artificial brookite.[15,16,36,37] Moreover, comparison with the Raman spectra of TiA(UP) and TiB(UP) showed a shift from 142.4 cm^{-1} for anatase to 151.8 cm^{-1} for brookite and the appearance of a shoulder at 127.6 cm^{-1}.[15] The multiple-peaks and the Raman shift further confirmed the high purity of the as-prepared brookite phase.

Table 1 also compares the measured BET surface area, pore size, and pore volume of the unpretreated TiO_2 with He-pretreated samples. For the unpretreated TiO_2, TiA(UP) had the highest BET specific surface area (145.6 m^2/g), almost twice as much as that of TiB(UP) and three times as much as that of TiR(UP). TiB(UP) displayed the largest pore size and pore volume, probably because of its nanocrystals' unique rod-shaped morphology that is described later in this paper. For the He-pretreated TiO_2 samples, the surface areas of TiA(He) and TiB(He) slightly increased while their average pore size and pore volume slightly decreased as compared to those of TiA(UP) and TiB(UP). By contrast, TiR(He) had a slightly decreased surface area but comparable pore size and pore volume as that of TiR(UP). These slight variations are likely attributed to the experimental uncertainties in BET measurements as well as the sampling errors from different batches of materials. On the other hand, the crystal sizes of the samples with and without He-pretreatment were very close. The results demonstrate that He treatment at a moderate temperature (220 °C) had only a minor effect on the textural properties of the three polymorphs.

3.2. Size and Morphology of TiO_2 Polymorphs. Since the XRD results showed that the crystal sizes and phases of TiO_2 were not significantly changed after He treatment at a moderate temperature, the particle sizes and morphologies of the pretreated and unpretreated samples were expected to be similar. Thus, only the pretreated Ti(He) samples were analyzed by TEM and HRTEM. For TiA(He), the TEM image in Figure 3a shows aggregates of fine nanoparticles, while the HRTEM image in Figure 3b clearly shows a well-faceted crystal with an interplanar spacing of around 0.350 nm that matches the anatase phase (101) plane.[10] The anatase particles are irregularly shaped hexagons, circles, or rectangles with an average size of ~9 nm. For TiR(He), short nanoellipses can be observed on the edges of the aggregated flower-like structures in Figure 3c. However, the elliptical rods with diameters of ~20 nm are randomly oriented. According to the HRTEM observations in Figure 3d, the interplanar spacing of 0.322 nm between the adjacent lattices corresponds to the distance between the (110) crystal plane of the rutile phase.[35,38]

As shown in Figure 3e, the nanorod-shaped TiB(He) was randomly dispersed with a length of approximately 100 nm and a diameter of 20 nm. The HRTEM image in Figure 3f shows clear one-dimensional lattice fringes of TiO_2 (lattice spacing = 0.344 nm) that is very close to the brookite TiO_2 (111) lattice spacing of 0.346 nm.[10,15] The nanorods also consisted of a short-range ordered phase with a mean interplanar spacing of 0.544 nm, which coincides with the distance between octahedron chains in brookite along the [001] axis.[38] In addition to the (111) and (001) planes, other families of facets are identifiable (See Supporting Information, Figure S2), such as the (202)-type surfaces and the kinematically forbidden (100) periodicities,[37] corresponding to lattice spacings of 0.227 and 0.921 nm, respectively. As shown in Figure 3f, some irregular shape particles with a smaller size (~ 5 nm) were observed on the top or edge of the brookite nanorods, and those particles might be amorphous TiO_2 as their lattice structure is not discernible.

3.3. Identification of Oxygen Vacancy and Ti^{3+} on Defective Surface. Figure 4 compares the UV−vis diffuse reflectance spectra, displayed in absorbance units, of the Ti(UP) and Ti(He) samples to identify the existence of defects induced by thermal treatment in He. The absorption edge of the Ti(UP) samples are obviously located at different positions around 400 nm, corresponding to a band gap of 3.11, 3.06, and 3.30 eV for TiA(UP), TiR(UP), and TiB(UP), respectively, close to the reported values of three phases TiO_2.[15,35] By contrast, TiA(He) and TiB(He) display similar tails extending to a longer wavelength of 600 nm, while TiR(He) exhibits an almost identical absorption profile as that of TiR(UP). Both theoretical and experimental UV−vis DRS results in the literature indicated that in the case of oxygen-deficient TiO_2, the broad band in the visible region of 450−600 nm was attributed to the light absorption of V_O, which can effectively harvest visible light and create a color center.[19,26,39,40] Hence, the red-shifts of TiA(He) and TiB(He) likely resulted from the formation of surface V_O. Similar UV−vis DRS results were reported in our previous study indicating that thermal pretreatment in He caused the formation of V_O on a Cu/TiO_2(P25) sample.[27] The almost identical absorption

dx.doi.org/10.1021/cs300273q | ACS Catal. 2012, 2, 1817−1828

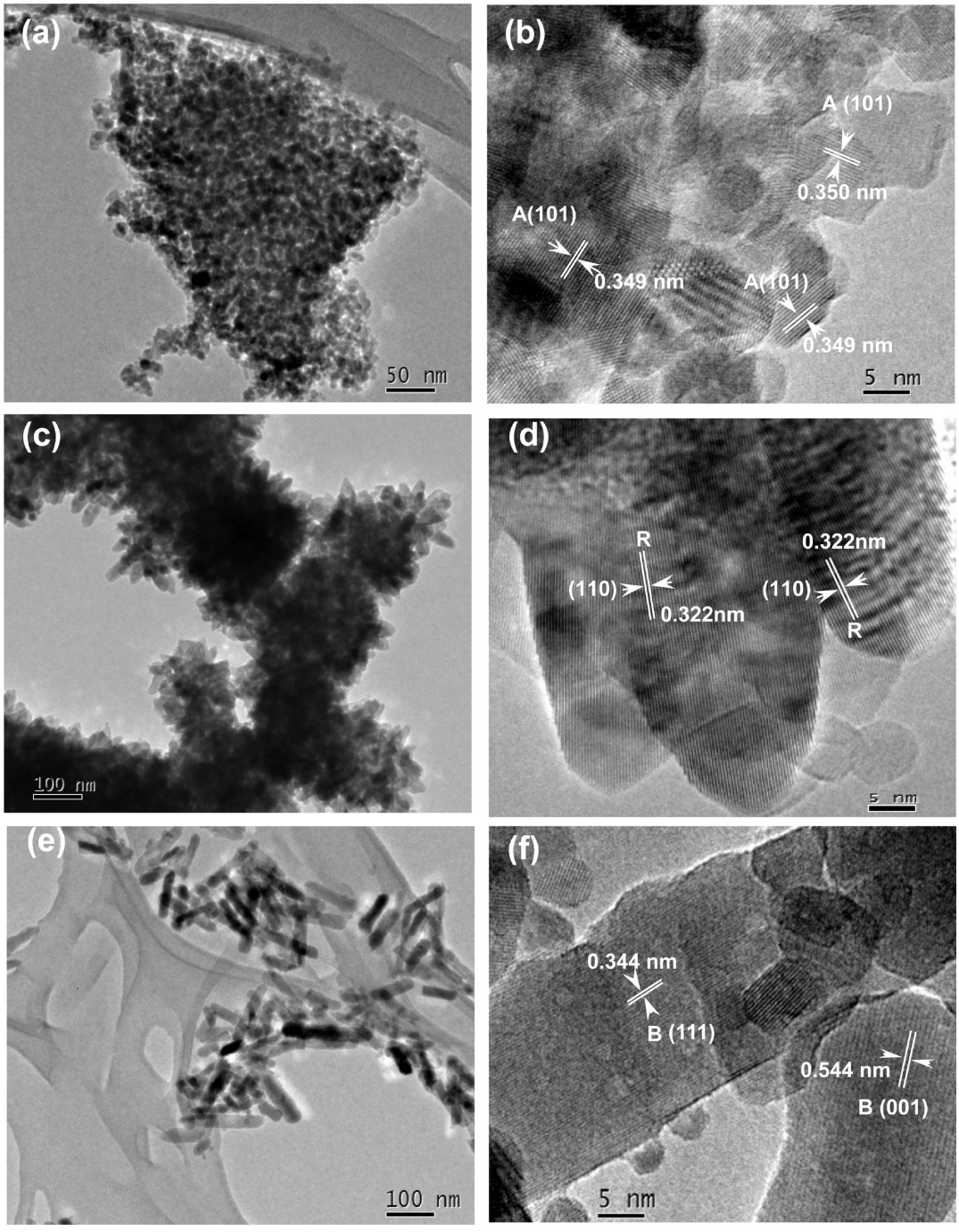

Figure 3. TEM and HRTEM images for (a, b) TiA(He), (c, d) TiR(He), and (e, f) TiB(He). HRTEM images were labeled with examples of anatase (A), rutile (R), and brookite (B).

profiles of TiR(UP) and TiR(He) in this work indicated the absence of V_O on the rutile phase. The existence of V_O was further supported by the different colors of the Ti(UP) and Ti(He). The colors of the three original Ti(UP) samples were white. After He pretreatment, the color of the TiA(He) changed to brownish-gray and that of TiB(He) changed to gray (see the inset pictures in Figure 4), while TiR(He) remained white. Chen et al.[20] prepared hydrogen-reduced TiO_2 with a black color, and they reported that the intrinsic defect disorders like V_O and Ti interstitial on their sample caused such appearance. The color change of TiO_2 in this work directly supports the conclusion of V_O formation on TiA(He) and TiB(He), whereas the three Ti(UP) samples and TiR(He) surface are relatively defect-free.

A comparison of the DRIFTS spectra of unpretreated and He-pretreated samples in the range of 3000−3800 cm^{-1} was used to elucidate the existence of Ti^{3+} species. As shown in Figure 5a, similar IR bands at 3693 and 3000−3600 cm^{-1} exist on TiA(UP), TiR(UP), and TiB(UP). These bands are assigned to the stretching vibration of H-bound OH groups and physically adsorbed H_2O, respectively.[41,42] By contrast, for Ti(He) samples as shown in Figure 5b, the original 3693 and 3000−3600 cm^{-1} bands disappeared or became significantly weakened, probably because of the desorption of weakly

dx.doi.org/10.1021/cs300273q | ACS Catal. 2012, 2, 1817−1828

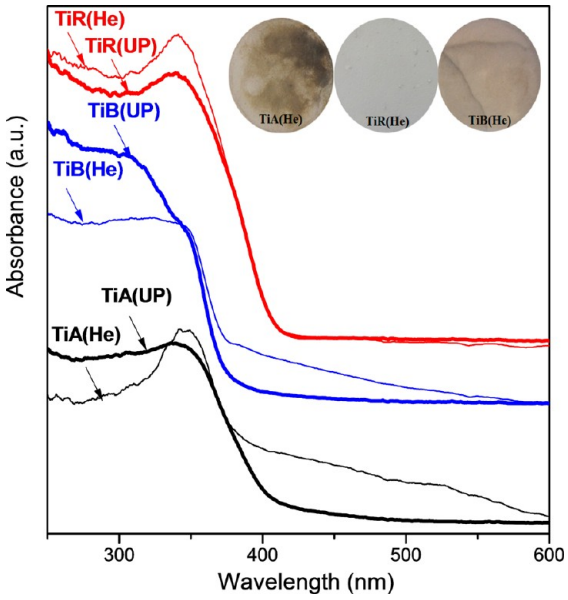

Figure 4. UV−visible diffuse reflectance spectra of unpretreated and He-pretreated TiO_2 (anatase, rutile, and brookite). The inset picture shows the color differences of the three TiO_2 polymophs after He-pretreatment.

bonded H_2O. Meanwhile, new bands appeared at 3415, 3650, 3678, and 3720 cm^{-1}, where the former three bands were assigned to Ti^{4+}−OH and the latter one was assigned to Ti^{3+}−OH.[41−44] This confirms that thermal pretreatment in He leads to the formation of Ti^{3+} on the Ti(He) surface because of the oxygen loss, which is in good agreement with the literature that indicated that annealing in an inert environment was likely to result in the partial reduction of Ti^{4+} to Ti^{3+} with the generation of surface V_O simultaneously, that is, $[Ti^{4+}-O-Ti^{4+}] \rightarrow [Ti^{3+}-\square-Ti^{3+}] + (1/2)O_2$.[18,19,22] On the other hand, the relative intensities of Ti^{3+}−OH on TiA(He) and TiB(He) are stronger than that on TiR(He). This difference suggested that the relative concentration of V_O/Ti^{3+} sites was likely in the order of TiA(He) ≈ TiB(He) > TiR(He), which is consistent with the previously presented UV−vis absorption results and the color differences noted for the three samples (Figure 4).

3.4. Activity of CO_2 Photoreduction. Background tests were first conducted with a mixture of He + H_2O passing through the TiO_2 catalyst under photoillumination; no carbon-containing products were detected. Photoreduction products (CO and CH_4) were observed only in the presence of CO_2, confirming CO_2 was indeed the carbon source. CH_4 is a valuable product and can be directly used as a fuel. CO is also an important chemical feedstock and an essential component of synthetic gas or syngas, a mixture of H_2 and CO. Syngas can be further converted to liquid hydrocarbon fuels through well-known Fischer-Tropcsh processes.[1,45,46] No reaction carbon-containing products other than CO and CH_4 were detected by the GC/TCD-FID used in this work.

By measuring the concentrations of CO and CH_4 at the reactor outlet, the production of CO and CH_4, in μmol g^{-1}, during a 6 h photoillumination period was calculated, and the data are shown in Figure 6. TiB(He) had the highest CO

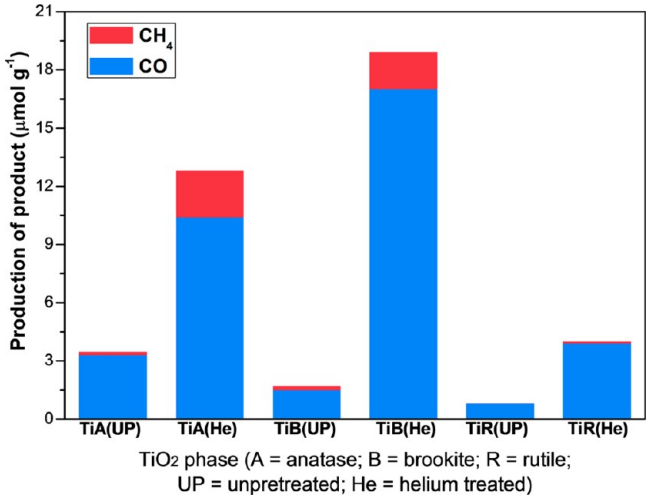

Figure 6. Production of CO and CH_4 on the three unpretreated and He pretreated TiO_2 polymorphs for a period of 6 h photoillumination.

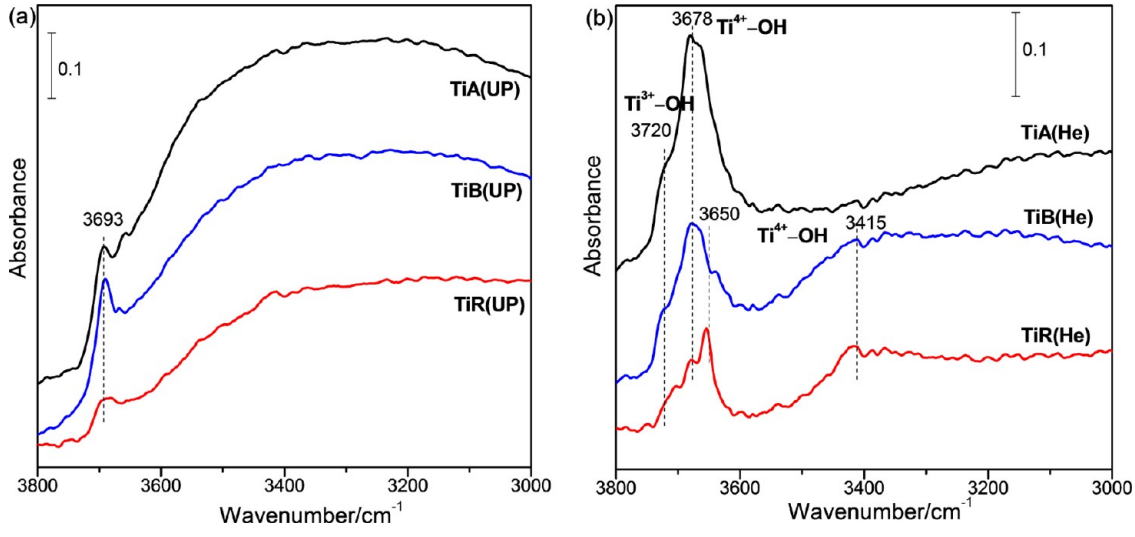

Figure 5. DRIFTS spectra of OH groups in the region of 3000−3800 cm^{-1} for (a) unpretreated and (b) pretreated TiO_2 samples (anatase, rutile, and brookite).

dx.doi.org/10.1021/cs300273q | ACS Catal. 2012, 2, 1817−1828

production among all the tested samples, and 50% higher than TiA(He). TiA(He) had the highest CH_4 production, but only slightly higher than TiB(He). The rutile samples, pretreated or not, were the least active ones. Compared to the unpretreated samples, the activity of the He-pretreated samples was enhanced by 2.2, 10.3, and 3.9 times for CO production and by 13.3, 8.2, and 5 times for CH_4 production on anatase, brookite, and rutile, respectively. It is clear that the factor of enhancement because of sample pretreatment was most significant on brookite (8−10 times), followed by anatase and rutile. The overall production of CO and CH_4 on TiB(He) and TiA(He) in this work was 18.9 and 12.8 μmol g^{-1}, respectively, much higher than those reported in the literature using bare TiO_2 for CO_2 photoreduction. Kočí et al.[5] reported a total production of CO, CH_4, and CH_3OH of about 2.9 μmol g^{-1} after 8 h photoreaction on an anatase TiO_2 sample. Dimitrijevic et al.[47] reported a production of only CH_4 about 0.37 μmol g^{-1} after 4 h photoreaction on a TiO_2−P25 sample. Clearly, our engineered catalysts developed in this work demonstrate a superior activity. This is an important experimental finding that for the first time in the literature reveals oxygen-deficient brookite TiO_2 as a more outstanding form than anatase and rutile for CO_2 photoreduction to CO and CH_4.

To investigate the feasibility of H_2 and O_2 production during the process of CO_2 photoreduction with H_2O, the concentration of H_2 and O_2 was monitored in a separate test using brookite as the catalyst. The possibility of H_2 production from H_2O splitting by photoirradiation was tested by switching the GC carrier gas from He to N_2 or Ar to enhance the sensitivity for H_2 detection. However, no matter whether using N_2 or Ar as GC carrier gas, still no H_2 was detected on either unpretreated or pretreated brookite, although H_2 production is thermodynamically feasible in theory. This result agrees with our previous published results that no H_2 was formed on an iodine-doped TiO_2 catalyst during CO_2 photoreduction with H_2O.[10] The literature also reported either no H_2 or trace H_2 production on bare TiO_2, with concentrations of H_2 much smaller than those of the CO_2 reduction products.[3,5] The H_2 production was prominent only in the presence of noble metal cocatalysts (e.g., Pt, Ag)[9,48] or in the presence of sacrificial agents (e.g., CH_3OH).[20,48] A recent study[49] using a Pt/TiO_2 thin-film catalyst for CO_2 photoreduction with H_2O reported only CO and CH_4 production without detection of H_2. On the basis of the literature results and our findings, we believe the absence of H_2 production in this work is possibly due to the following reasons: (1) the lack of noble metal cocatalysts to lower the activation barrier for H_2 production; (2) protons or •H radicals formed by the photodissociation of water is competitively consumed by CO_2 reduction intermediates like CO_2^- to produce CO and CH_4; and (3) the produced H_2, if any, can be consumed by backward reactions with CO or O_2.

The measurement of possible O_2 production from H_2O oxidation was investigated using pretreated brookite, that is, TiB(He). Before turning on the UV−vis illumination, the photoreactor was purged with a CO_2−H_2O mixture flow to eliminate the air inside the reactor. However, there was always background O_2 and N_2 in the order of a few hundred ppm detected in the reactor effluent gas even after purging for a few hours. Hence, a better indicator of O_2 production by the catalyst during the photoreaction is the volumetric ratio of O_2/N_2 in the effluent gas, as also suggested in our previous work.[10,13] Figure 7 shows the O_2/N_2 ratio before, during, and after the photoreaction, when gas sampling was conducted

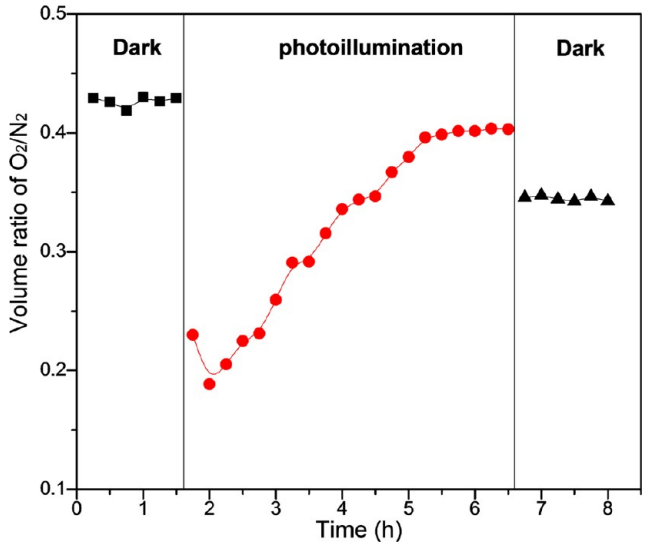

Figure 7. Time dependence of the volumetric ratio of O_2/N_2 before, during, and after the photoreduction of CO_2 with H_2O on the TiB(He).

every 15 min. Before the photoillumination (in the dark), the O_2/N_2 ratio was steady. Interestingly, immediately upon photoillumination, the O_2/N_2 ratio dramatically decreased in the first 30 min and then gradually increased thereafter. This sharp decrease is possibly caused by the consumption of residual O_2 in the reactor through the reaction with photogenerated electrons $O_2 + e^- \rightarrow O_2^-$ and consecutive reactions.[13,14] The gradual increase in the O_2/N_2 ratio after the 30 min photoillumination suggested the generation of O_2 through oxidation of H_2O by photogenerated holes, $H_2O + 2\ h^+ \rightarrow 2H^+ + (1/2)O_2$. This O_2 generation process overweighed the previous mentioned concurrent O_2 consumption process, and thus, the net result was that the O_2/N_2 ratio increased gradually with time and finally stabilized after 6 h when the generation/consumption processes reached equilibrium. When the light was turned off (the second dark period), an obvious drop in the O_2/N_2 ratio was observed. This result again verified that there was O_2 generated during the photocatalytic CO_2 reduction process.

3.5. In Situ DRIFTS for CO_2 Photoreduction. The photoreduction data indicated that pretreated surfaces were more active that unpretreated ones. To further verify the role of V_O/Ti^{3+} sites on the pretreated surface, in situ DRIFTS studies of CO_2 photoreduction with H_2O were performed on defect-free TiA(UP) and TiB(UP), as well as defective TiA(He) and TiB(He). Figure 8 shows the IR spectra of CO_2 and H_2O co-interaction with TiA(UP) and TiB(UP). In the dark, TiA(UP) and TiB(UP) surfaces were dominated by strongly adsorbed H_2O at 1647 cm^{-1}, weak bicarbonate (HCO_3^-) features at 1420−1428 and 1221 cm^{-1}, and bidentate or monodentate carbonates (b-CO_3^{2-}, m-CO_3^{2-}) at 1500−1590 cm^{-1}.[31,32,36] Under subsequent photoillumination, the IR features for CO_2-related species and H_2O were almost identical to those in the dark, even after 60 min of illumination. No CO_2^- or other new species were formed, and the adsorbed H_2O was stable, indicating the difficulty in activating CO_2 and H_2O on irradiated TiA(UP) and TiB(UP).

Significantly different results were obtained on TiA(He) and TiB(He) surfaces under the same experimental conditions. As shown in Figure 9a, exposure of TiA(He) to CO_2 and H_2O in

dx.doi.org/10.1021/cs300273q | ACS Catal. 2012, 2, 1817−1828

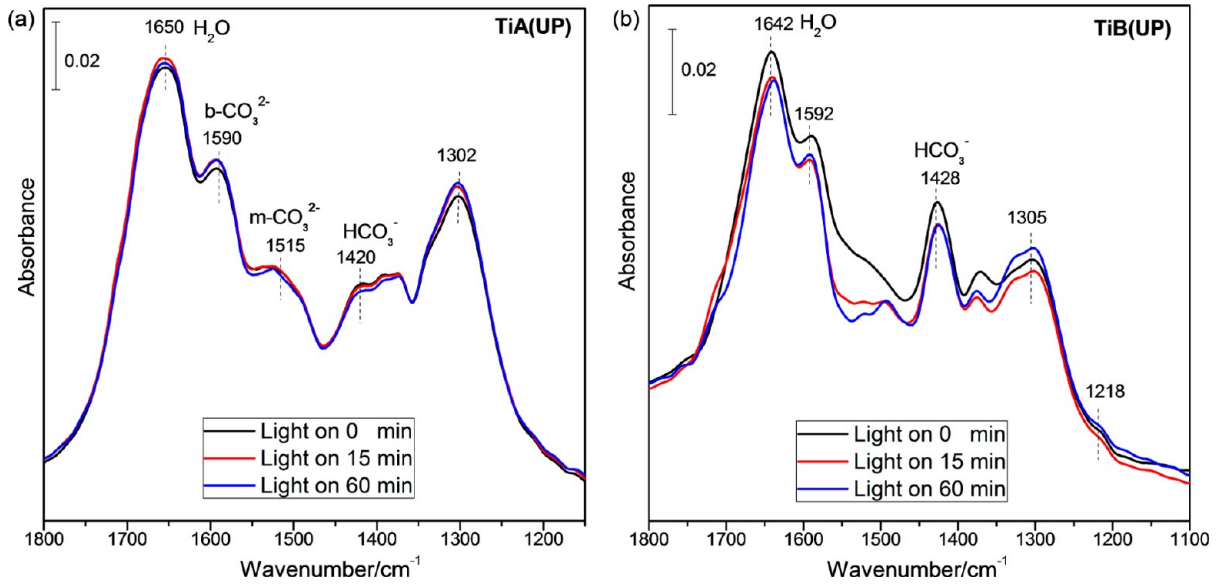

Figure 8. In situ DRIFTS spectra of CO_2 and H_2O interaction with (a) TiA(UP) and (b) TiB(UP) irradiated by UV−visible light as a function of time. The light was turned on after the samples sat in the dark for 15 min.

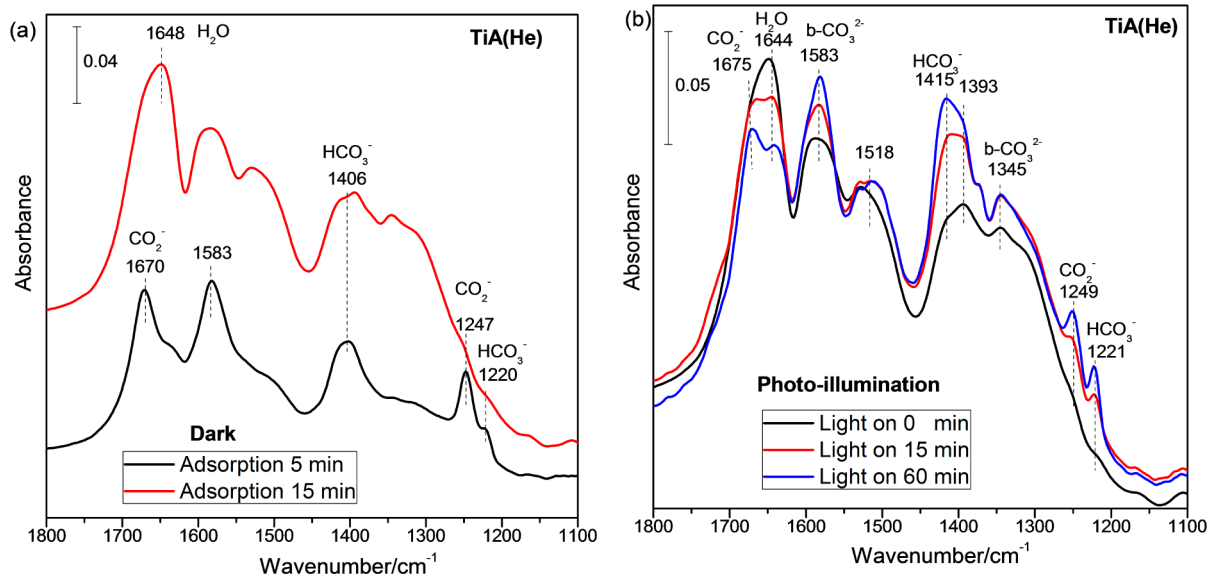

Figure 9. In situ DRIFTS spectra of CO_2 and H_2O interaction with TiA(He) (a) in the dark, and (b) subsequently irradiated by UV−visible light as a function of time.

the dark led to the rapid formation of CO_2^-, HCO_3^-, and b-CO_3^{2-} species in the initial 0−5 min time frame. The formation of $Ti^{4+}-CO_2^-$ indicates that an electron could be spontaneously attached to CO_2 from defective anatase even in the dark. The vibrational frequency of CO_2^- in this work (at 1670 and 1247 cm^{-1}) correlated well with the experimental values reported in the literature[30,36] as well as the calculated values of CO_2 adsorbed on an oxygen-deficient anatase (101) plane.[24] Prolonging the time to 15 min in the dark resulted in the disappearance of CO_2^- and a gradual decrease of HCO_3^- and b-CO_3^{2-}, but an increase in the intensity of the H_2O band. This result suggests that CO_2 and H_2O may compete for the same defect sites; H_2O could replace the adsorbed CO_2^- species and partially substitute HCO_3^- by occupying the V_O/Ti^{3+} sites and OH groups. This replacement possibly results from the higher binding energy of H_2O with TiO_2 than that of CO_2.[21,24,29]

As shown in Figure 9b, photoillumination apparently induced the reappearance of CO_2^- (1675 and 1249 cm^{-1}) on the TiA(He) surface. Meanwhile, the intensities of the IR spectral features for HCO_3^- (1415 and 1221 cm^{-1}) and b-CO_3^{2-} (1583 and 1345 cm^{-1}) increased with prolonged irradiation time, but that for adsorbed H_2O decreased. This is a strong evidence that unlike TiA(UP), the TiA(He) surface allowed the photoexcited electrons that were trapped in the defect sites to transfer to the adsorbed CO_2, although the literature indicates the difficulty or impossibility of one-electron reduction of CO_2 on TiO_2.[2,47] To verify whether the spectral change (i.e., reappearance of CO_2^-) could be caused by the readsorption of CO_2 by dehydration, an additional experiment was conducted under the following conditions in sequence: (1) preadsorption of H_2O vapor on TiA(He) in the dark, (2) photoirradiating the TiA(He) surface for 1 h, and (3) turning off the light and introducing CO_2 to

dx.doi.org/10.1021/cs300273q | ACS Catal. 2012, 2, 1817−1828

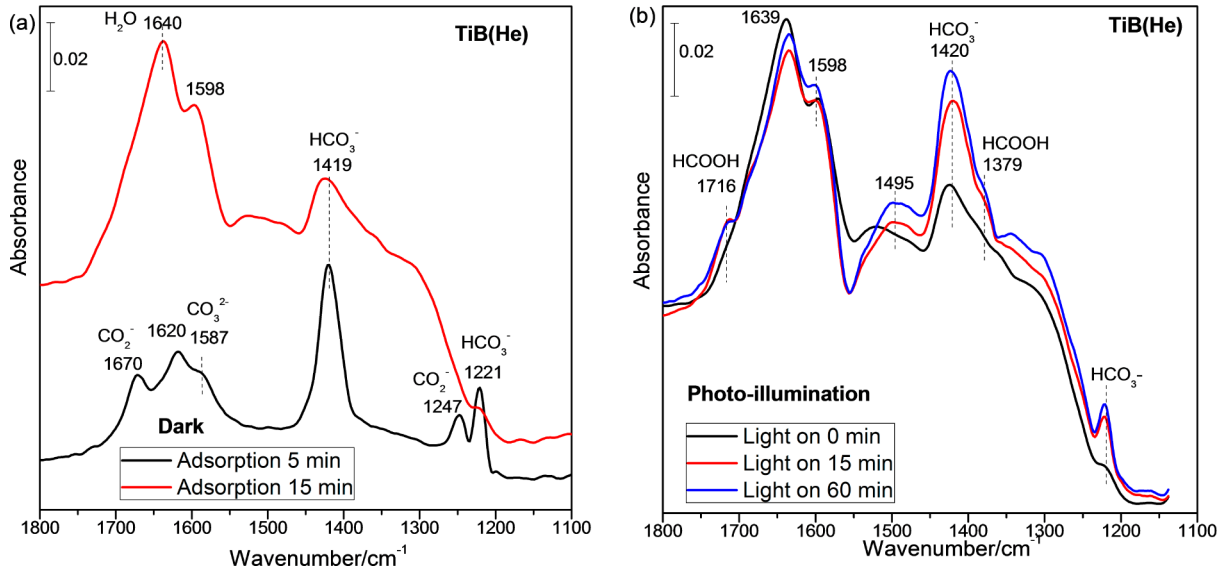

Figure 10. In situ DRIFTS spectra of CO_2 and H_2O interaction with TiB(He) (a) in the dark, and (b) subsequently irradiated by UV−visible light as a function of time.

Table 2. Possible Reaction Pathways for the Formation of CO and CH_4 from CO_2 Photoreduction with H_2O Vapor on Oxygen-Deficient TiO_2 Anatase and Brookite Phases

phase	CO_2 photoreduction with H_2O vapor	
defective TiO_2 anatase and brookite	$H_2O + h^+ \rightarrow H^+ + OH\bullet$ (1)	$CO_2 + Ti^{3+} \rightarrow Ti^{4+}-CO_2^-$ (2)
	$OH\bullet + CO_2^- \rightarrow HCO_3^-$ (3)	$CO_2^- + H^+ + e^- \rightarrow CO + OH^-$ (4)
	$CO_2^- + CO_2^- \rightarrow CO + CO_3^{2-}$ (5)	$CO_2^- + [Ti^{3+}-V_O-Ti^{4+}] \rightarrow CO + [Ti^{4+}-O^{2-}-Ti^{4+}]$ (6)
	$CO, HCO_3^-, HCOOH \xrightarrow{e^-} C_{(ads)}\cdot \xrightarrow{H\bullet} CH_3\cdot \xrightarrow{H\bullet} CH_4$ (7)	
defective TiO_2 brookite	$CO_2 + 2H^+ + 2e^- \rightarrow HCOOH$ (8)	$CO_2^- + 2H^+ + e^- \rightarrow HCOOH$ (9)
	$HCOOH \rightarrow CO + H_2O$ (10)	$CO, HCOOH \xrightarrow{e^-,H^+} CH_4$ (11)

TiA(He). It was found that photoirradiation (step 2) led to surface dehydration to some extent (by observation of reduced H_2O adsorption band intensity), but the subsequent CO_2 adsorption in the dark (step 3) on the dehydrated surface did not result in the occurrence of CO_2^- and HCO_3^- species. The above result verified that the reappearance of CO_2^- in Figure 9b was due to the photoinduced activation and reduction of CO_2 but not due to the readsorption of CO_2. These spectral changes in Figure 9 also suggest that the three carbon-containing species (CO_2^-, HCO_3^- and b-CO_3^{2-}) may be the primary intermediates on the treated anatase surface during the CO_2 photoreduction process, and H_2O participates in the reaction with CO_2 by donating electrons or scavenging holes.

Figure 10 shows CO_2 and H_2O co-interaction with TiB(He) in the dark and under photoillumination. Similar to the features observed on TiA(He), H_2O partially substituted the CO_2^-, HCO_3^-, and CO_3^{2-} in the dark (Figure 10a), and photoexcitation of TiB(He) surface induced a remarkable reappearance of HCO_3^- with a concurrent slight decrease of H_2O (Figure 10b). However, a reappearance of CO_2^- was not observed. Rather, two new bands at 1716 and 1379 cm^{-1} attributed to formic acid (HCOOH)[50] occurred under photoillumination. This suggests that CO_2^-, HCO_3^-, and HCOOH are possibly the major intermediates on the TiB(He) surface. It is also noted that a new broad band at 1495 cm^{-1} appeared on TiB(He), and its intensity increased with the irradiation time. The IR study of CO adsorption on Cu(I)/TiO_2 by Yang et al.[32] suggested that a similar band at 1492 cm^{-1} was indicative of CO adsorbed on Ti(O) sites as bicarbonates. Hence, this 1495 cm^{-1} band may originate from the adsorption of the CO product.

4. DISCUSSION

4.1. CO_2 Photoreduction Mechanism on Anatase and Brookite. On the basis of the photoactivity data and in situ DRIFTS observations, we proposed a tentative mechanism for CO and CH_4 formation from CO_2 photoreduction with H_2O on defective anatase and brookite TiO_2, as expressed in Reactions 1−11 in Table 2. The IR results in Figures 9 and 10 demonstrate the dissociation of H_2O (Reaction 1) and the generation of CO_2^- (Reaction 2) and HCO_3^- (Reaction 3) intermediates on both the TiA(He) and TiB(He) surfaces. In agreement with the mechanism reported in the literature,[5,30,33,47,51] CO_2^- could be reduced to CO via reaction with H^+ (Reaction 4) or self-transformation (Reaction 5), or direct dissociation by healing the V_O sites (Reaction 6).

It is worth noting that unlike what occurs on TiA(He), CO_2^- was not present on TiB(He) under photoillumination in the presence of H_2O (Figure 10b). This is likely due to the faster reaction of CO_2^- with H^+ (generated from H_2O) to produce CO (Reaction 4) on TiB(He) than on TiA(He). This conclusion was supported by additional experimental results

dx.doi.org/10.1021/cs300273q | ACS Catal. 2012, 2, 1817−1828

obtained under the condition where CO_2 in the absence of H_2O vapor was allowed to interact with Ti(He) (see Supporting Information, Figure S3). CO_2^- appeared on TiB(He) even without H_2O vapor and its intensity increased with illumination time (Supporting Information, Figure S3b). This may be a result of the photoreduction of adsorbed CO_2 with OH groups on the "dry" surface. The TiB(He) surface is favorable for adsorbed H_2O (or OH groups or H^+ species) to quickly scavenge CO_2^- and produce CO so that no CO_2^- could be observed on TiB(He) under illumination (Figure 10b). By contrast, the CO_2^- intensity on TiA(He) neither increased nor disappeared under illumination in the absence of H_2O vapor (Supporting Information, Figure S3a), suggesting a low reaction rate of CO_2^- with OH groups or H^+ species on the TiA(He) surface. Furthermore, the photoactivity data (Figure 6) also indicate the superior activity of TiB(He) as compared to TiA(He) for CO production. Hence, the DRIFTS and photoactivity results correlate well with each other and clearly demonstrate that defective brookite is more active than anatase in facilitating the reaction of CO_2^- with H_2O.

In addition, IR results in Figures 9 and 10 show the formation of HCOOH on TiB(He) but not on TiA(He). HCOOH may originate from the reaction of CO_2 or CO_2^- with two H^+ and electrons (Reactions 8 and 9, Table 2). Ulagappan et al.[50] pointed out that HCOOH, generated by CO_2 photoreaction with methanol on Ti-silica sieve, could be photodissociated into CO and H_2O. Similar dissociation of HCOOH to CO may occur on the TiB(He) surface (Reaction 10, Table 2). This unique reaction on TiB(He) indicates that CO_2 photoreduction to CO probably undergoes different mechanisms on defective anatase and brookite phases through different surface intermediates (e.g., CO_2^- on anatase; CO_2^-, and HCOOH on brookite).

Regarding the reaction pathway for CH_4 formation, we propose that the carbon-containing intermediates such as CO, surface HCO_3^- and HCOOH may be converted to CH_4 via a multielectron transfer process, once dissociated hydrogen atoms are available (Reactions 7 and 11, Table 2).[13,14,45,47,52] It is also possible for CH_4 to decompose through reaction with photogenerated OH radicals to form CO. These two factors may contribute to the finding that the production of CH_4 was always lower than the production of CO determined in this work. Further investigation of the more complicated CH_4 formation mechanism involving an eight-electron transfer process will be in the scope of our future study.

4.2. Role of Oxygen Vacancy and Ti^{3+}. It is important to understand why the photoactivity for CO_2 reduction was enhanced on the defective surface. The effects of crystal structure, particle size, and morphology can be excluded because the XRD, TEM, and HRTEM analyses did not indicate significant changes between the unpretreated and pretreated samples. Ultimately, the UV−vis, physical color, and IR studies show apparent evidence for the formation of reactive V_O/Ti^{3+} sites on Ti(He) surface. In situ DRIFTS results in Figures 8−10 demonstrate the more favorable formation of briged-CO_2^-, HCO_3^-, or HCOOH and the dissociation of H_2O on oxygen-deficient Ti(He) rather than on defect-free Ti(UP), which confirms that the V_O/Ti^{3+} defects, as "local factors", could readily provide reactive sites for the adsorption of reactants and allow effective charge or hole transfer between CO_2/H_2O and the TiO_{2-x} surface under photoillumination.

It is noted that for unpretreated samples like TiA(UP) and TiB(UP), although CO_2^- was not detected under photoillumination (Figure 8), their activity in CO_2 photoreduction was recorded by the GC measurement (Figure 6). The absence of CO_2^- in the DRIFTS measurement for the TiA(UP) and TiB(UP) samples may have two reasons. First, the catalyst area that was exposed to irradiation was approximately 40 times smaller in the DRIFTS reaction cell than in the flow reactor. Thus, a much smaller amount of CO_2^- was formed in the DRIFT cell. Second, the kinetics of CO_2^- transition to CO may be fast so that CO_2^- may not be detectable if in small quantity. The detection of CO_2^- on the pretreated samples, such as TiA(He), clearly reveals their higher activities in CO_2 photoreduction because of the presence of V_O/Ti^{3+} defects.

4.3. Phase-Dependent Photoefficiency on Defective TiO_2. The surface area may have a minor effect on phase-dependent photoefficiency, since the activity of TiB(He) was higher than that of TiA(He) even though TiB(He) had a lower surface area (87.8 m^2/g) than TiA(He) (163.8 m^2/g, Table 1). There are two possible major reasons why the defective brookite phase resulted in higher combined production for CO and CH_4 as compared to the production using anatase and rutile. First, the results in Figures 4 and 5 suggest that the relative concentration of V_O/Ti^{3+} are comparable on the anatase and brookite surfaces, but are negligible on the rutile surface. This is in agreement with the theoretical results that the lower formation energy of V_O on brookite (5.52 eV) and anatase (5.58 eV) may facilitate the creation of V_O on these surfaces as compared to the rutile surface (5.82 eV).[23] This difference accounts for the much higher activity on defective brookite and anatase than on rutile.

Second, surface reaction intermediates may influence the photoactivity.[14] Published studies proposed that the initial key step for the photoreduction of CO_2 was the formation of CO_2^- intermediates.[24,30,33,51] Rasko et al.[30] also demonstrated that a bent-CO_2^- was transformed into CO on prereduced Rh/TiO_2. According to this analysis, the different behaviors of CO_2^- on TiO_2 may lead to a divergence in the activity between anatase and brookite. The mechanism discussion in Section 4.1 indicates that CO_2^- on TiB(He) is more likely to react with H^+ than that on TiA(He), and that HCOOH is another possible intermediate on TiB(He). The added routes of HCOOH to CO and CH_4 may also contribute to the higher overall production of CO and CH_4 on defective brookite than on anatase.

5. CONCLUSIONS

This work combined in situ DRIFTS and photoactivity measurements to comparatively study CO_2 photoreduction with H_2O vapor on defect-free and oxygen-deficient TiO_2 nanocrystals. The photoactivity of defective TiO_2 was remarkably higher than that of defect-free TiO_2. This enhancement was primarily attributed to the creation of oxygen vacancies and Ti^{3+} on the surface, which could promote CO_2 activation both in the dark and under photoillumination by generating CO_2^- intermediates. Another important finding was that for TiO_2 surfaces engineered with defect sites, brookite, the least studied structure among the three TiO_2 polymorphs, had the highest yield for CO and CH_4 production, followed by anatase and rutile. Possible reasons for this superior activity of defective brookite include the facilitated formation of oxygen vacancies, faster reaction rate of CO_2^- with adsorbed H_2O or surface OH groups, and an additional reaction route involving an HCOOH intermediate. This study has provided new information to correlate the surface chemistry (defect sites,

reaction intermediates) with CO_2 reduction activity by TiO_2. The brookite phase appears to be a promising material for CO_2 reduction, and therefore warrants further research along this topic, including the investigation of brookite-containing mixed phases. This work is currently underway.

■ ASSOCIATED CONTENT

Supporting Information

The irradiation spectrum of solar simulator used in this work, HRTEM image of He pretreated brookite TiO_2, and the in situ DRIFTS spectra of CO_2 interaction with pretreated anatase and brookite TiO_2 in the dark and under photoirradiation. This material is available free of charge via the Internet at http://pubs.acs.org.

■ AUTHOR INFORMATION

Corresponding Author

*Phone: (+1) 414-229-3716. Fax: (+1) 414-229-6958. E-mail: liying@uwm.edu.

Funding

This work was supported by the National Science Foundation Division of Chemical, Bioengineering, Environmental, and Transport Systems (CBET-1067233 and CBET-1067340).

Notes

The authors declare no competing financial interest.

■ ACKNOWLEDGMENTS

The authors also acknowledge Donald Robertson at the Physics Laboratory for High Resolution Transmission Electron Microscopy at UW-Milwaukee for his assistance in TEM and HRTEM analyses.

■ REFERENCES

(1) Roy, S. C.; Varghese, O. K.; Paulose, M.; Grimes, C. A. *ACS Nano* **2010**, *4* (3), 1259−1278.
(2) Indrakanti, V. P.; Kubicki, J. D.; Schobert, H. H. *Energy Environ. Sci.* **2009**, *2* (7), 745−758.
(3) Anpo, M.; Yamashita, H.; Ichihashi, Y.; Ehara, S. *J. Electroanal. Chem.* **1995**, *396* (1−2), 21−26.
(4) Saladin, F.; Forss, L.; Kamber, I. *J. Chem. Soc., Chem. Commun.* **1995**, *5*, 533−534.
(5) Kočí, K.; Obalova, L.; Matejova, L.; Placha, D.; Lacny, Z.; Jirkovsky, J.; Solcova, O. *Appl. Catal., B* **2009**, *89* (3−4), 494−502.
(6) Saladin, F.; Alxneit, I. *J. Chem. Soc., Faraday Trans.* **1997**, *93* (23), 4159−4163.
(7) Tseng, I. H.; Chang, W. C.; Wu, J. C. S. *Appl. Catal., B* **2002**, *37* (1), 37−48.
(8) Li, G. H.; Gray, K. A. *Chem. Phys.* **2007**, *339* (1−3), 173−187.
(9) Varghese, O. K.; Paulose, M.; LaTempa, T. J.; Grimes, C. A. *Nano Lett.* **2009**, *9* (2), 731−737.
(10) Zhang, Q. Y.; Li, Y.; Ackerman, E. A.; Gajdardziska-Josifovska, M.; Li, H. L. *Appl. Catal., A* **2011**, *400* (1−2), 195−202.
(11) Tseng, I. H.; Wu, J. C. S.; Chou, H. Y. *J. Catal.* **2004**, *221* (2), 432−440.
(12) Mor, G. K.; Varghese, O. K.; Wilke, R. H. T.; Sharma, S.; Shankar, K.; Latempa, T. J.; Choi, K. S.; Grimes, C. A. *Nano Lett.* **2008**, *8* (7), 1906−1911.
(13) Li, Y.; Wang, W. N.; Zhan, Z. L.; Woo, M. H.; Wu, C. Y.; Biswas, P. *Appl. Catal., B* **2010**, *100* (1−2), 386−392.
(14) Yang, C. C.; Vernimmen, J.; Meynen, V.; Cool, P.; Mul, G. *J. Catal.* **2011**, *284* (1), 1−8.
(15) Kandiel, T. A.; Feldhoff, A.; Robben, L.; Dillert, R.; Bahnemann, D. W. *Chem. Mater.* **2010**, *22* (6), 2050−2060.
(16) Li, J. G.; Ishigaki, T.; Sun, X. D. *J. Phys. Chem. C* **2007**, *111* (13), 4969−4976.
(17) Chiarello, G. L.; Di Paola, A.; Palmisano, L.; Selli, E. *Photochem. Photobiol. Sci.* **2011**, *10* (3), 355−360.
(18) Nowotny, M. K.; Sheppard, L. R.; Bak, T.; Nowotny, J. *J. Phys. Chem. C* **2008**, *112* (14), 5275−5300.
(19) Danon, A.; Bhattacharyya, K.; Vijayan, B. K.; Lu, J. L.; Sauter, D. J.; Gray, K. A.; Stair, P. C.; Weitz, E. *ACS Catal.* **2012**, *2* (1), 45−49.
(20) Chen, X. B.; Liu, L.; Yu, P. Y.; Mao, S. S. *Science* **2011**, *331* (6018), 746−750.
(21) Aschauer, U.; He, Y. B.; Cheng, H. Z.; Li, S. C.; Diebold, U.; Selloni, A. *J. Phys. Chem. C* **2010**, *114* (2), 1278−1284.
(22) Deskins, N. A.; Rousseau, R.; Dupuis, M. *J. Phys. Chem. C* **2010**, *114* (13), 5891−5897.
(23) Pan, H.; Gu, B. H.; Zhang, Z. Y. *J. Chem. Theory Comput.* **2009**, *5* (11), 3074−3078.
(24) He, H. Y.; Zapol, P.; Curtiss, L. A. *J. Phys. Chem. C* **2010**, *114* (49), 21474−21481.
(25) Sutter, P.; Acharya, D. P.; Camillone, N. *J. Phys. Chem. C* **2011**, *115* (24), 12095−12105.
(26) DeSario, P. A.; Chen, L.; Graham, M. E.; Gray, K. A. *J. Vac. Sci. Technol. A* **2011**, *29* (3), 0315081−0315087.
(27) Liu, L. J.; Zhao, C. Y.; Li, Y. *J. Phys. Chem. C* **2012**, *116* (14), 7904−7912.
(28) Indrakanti, V. P.; Kubicki, J. D.; Schobert, H. H. *Fuel Process. Technol.* **2011**, *92* (4), 805−811.
(29) Selloni, A.; Sun, C. H.; Liu, L. M.; Lu, G. Q.; Smith, S. C. *J. Mater. Chem.* **2010**, *20* (46), 10319−10334.
(30) Rasko, J.; Solymosi, F. *J. Phys. Chem.* **1994**, *98* (29), 7147−7152.
(31) Baltrusaitis, J.; Schuttlefield, J.; Zeitler, E.; Grassian, V. H. *Chem. Eng. J.* **2011**, *170* (2−3), 471−481.
(32) Yang, C. C.; Mul, G.; Yu, Y. H.; van der Linden, B.; Wu, J. C. S. *J. Am. Chem. Soc.* **2010**, *132* (24), 8398−8406.
(33) Lee, J.; Sorescu, D. C.; Deng, X. Y. *J. Am. Chem. Soc.* **2011**, *133* (26), 10066−10069.
(34) Kubicki, J. D.; Indrakanti, V. P.; Schobert, H. H. *Energy Fuels* **2009**, *23*, 5247−5256.
(35) Zhang, L. Z.; Wang, Y. W.; Deng, K. J.; Chen, X. Y.; Zou, Z. G. *J. Phys. Chem. C* **2007**, *111* (6), 2709−2714.
(36) Su, W. G.; Zhang, J.; Feng, Z. C.; Chen, T.; Ying, P. L.; Li, C. *J. Phys. Chem. C* **2008**, *112* (20), 7710−7716.
(37) Buonsanti, R.; Grillo, V.; Carlino, E.; Giannini, C.; Kipp, T.; Cingolani, R.; Cozzoli, P. D. *J. Am. Chem. Soc.* **2008**, *130* (33), 11223−11233.
(38) Reyes-Coronado, D.; Rodriguez-Gattorno, G.; Espinosa-Pesqueira, M. E.; Cab, C.; de Coss, R.; Oskam, G. *Nanotechnology* **2008**, *19* (14), 145605.
(39) Martyanov, I. N.; Uma, S.; Rodrigues, S.; Klabunde, K. J. *Chem. Commun.* **2004**, *21*, 2476−2477.
(40) Lin, Z. S.; Orlov, A.; Lambert, R. M.; Payne, M. C. *J. Phys. Chem. B* **2005**, *109* (44), 20948−20952.
(41) Glisenti, A.; Ferretto, L. *Chem. Mater.* **2003**, *15* (5), 1181−1188.
(42) Morterra, C. *J. Chem. Soc., Faraday Trans.* **1988**, *84* (5), 1617−1637.
(43) Martra, G. *Appl. Catal., A* **2000**, *200* (1−1), 275−285.
(44) Szczepankiewicz, S. H.; Colussi, A. J.; Hoffmann, M. R. *J. Phys. Chem. B* **2000**, *104* (42), 9842−9850.
(45) Uner, D.; Oymak, M. M. *Catal. Today* **2012**, *181* (1), 82−88.
(46) Ning, W. S.; Koizumi, N.; Yamada, M. *Energy Fuels* **2009**, *23*, 4696−4700.
(47) Dimitrijevic, N. M.; Vijayan, B. K.; Poluektov, O. G.; Rajh, T.; Gray, K. A.; He, H. Y.; Zapol, P. *J. Am. Chem. Soc.* **2011**, *133* (11), 3964−3971.
(48) Zhao, C. Y.; Krall, A.; Zhao, H. L.; Zhang, Q. Y.; Li, Y. *Int. J. Hydrogen Energy* **2012**, *37*, 9967−9976.
(49) Wang, W. N.; An, W. J.; Ramalingam, B.; Mukherjee, S.; Niedzwiedzki, D. M.; Gangopadhyay, S.; Biswas, P. *J. Am. Chem. Soc.* **2012**, *134*, 11276−11281.
(50) Ulagappan, N.; Frei, H. *J. Phys. Chem. A* **2000**, *104* (33), 7834−7839.

(51) Pipornpong, W.; Wanbayor, R.; Ruangpornvisuti, V. *Appl. Surf. Sci.* **2011**, *257* (24), 10322−10328.
(52) Zhang, Q. Y.; Gao, T. T.; Andino, J. M.; Li, Y. *Appl. Catal., B* **2012**, *123*−*124*, 257−264.